

TAIL: A Terrain-Aware Multi-Modal SLAM Dataset for Robot Locomotion in Deformable Granular Environments

Chen Yao^{*1}, Yangtao Ge^{*1}, Guowei Shi^{*1}, Zirui Wang^{*1}, Ningbo Yang¹, Zheng Zhu¹, Hexiang Wei², Yuntian Zhao¹, Jing Wu¹, Zhenzhong Jia^{1**}

Abstract—Terrain-aware perception holds the potential to improve the robustness and accuracy of autonomous robot navigation in the wilds, thereby facilitating effective off-road traversals. However, the lack of multi-modal perception across various motion patterns hinders the solutions of Simultaneous Localization and Mapping (SLAM), especially when confronting non-geometric hazards in demanding landscapes. In this paper, we first propose a Terrain-Aware multi-modal (TAIL) dataset tailored to deformable and sandy terrains. It incorporates various types of robotic proprioception and distinct ground interactions for the unique challenges and benchmark of multi-sensor fusion SLAM. The versatile sensor suite comprises stereo frame cameras, multiple ground-pointing RGB-D cameras, a rotating 3D LiDAR, an IMU, and an RTK device. This ensemble is hardware-synchronized, well-calibrated, and self-contained. Utilizing both wheeled and quadrupedal locomotion, we efficiently collect comprehensive sequences to capture rich unstructured scenarios. It spans the spectrum of scope, terrain interactions, scene changes, ground-level properties, and dynamic robot characteristics. We benchmark several state-of-the-art SLAM methods against ground truth and provide performance validations. Corresponding challenges and limitations are also reported. All associated resources are accessible upon request at <https://tailrobot.github.io/>.

Index Terms—SLAM dataset, multi-modal sensor fusion, different types of robots, deformable granular environments.

I. INTRODUCTION

Autonomous robotic platforms have been widely applied in outdoor missions such as exploration due to their promising mobility and reliability. However, these scientific-rich regions are often covered with rugged off-road terrains, which could lead to traversal hazards like sinkage or slippage, especially in deformable, granular scenes [1], [2]. Recognizing this, terrain-aware technologies are gaining popularity, empowering various robots to explore unexpected fields and providing reliable solutions for traversing uncertain risks. Multi-sensor fusion holds strong potential in enabling safe terrain traversal for field robotic applications. Integrating multi-modal data would ensure accurate and robust

¹Shenzhen Key Laboratory of Biomimetic Robotics and Intelligent Systems, Department of Mechanical and Energy Engineering, Southern University of Science and Technology (SUSTech), Shenzhen, 518055, China. Guangdong Provincial Key Laboratory of Human-Augmentation and Rehabilitation Robotics in Universities, SUSTech, Shenzhen, 518055, China.

²The Hong Kong University of Science and Technology (Guangzhou), Nansha, Guangzhou, 511400, Guangdong, China.

This work was supported in part by the Guangdong Natural Science Fund-General Programme under grant no. 2021A1515012384, the Science, Technology and Innovation Commission of Shenzhen Municipality under grant no. ZDSYS20200811143601004, and the National Science Foundation of China(NSFC)U1913603.

*Equal contribution.

**Corresponding author: jjazz@sustech.edu.cn

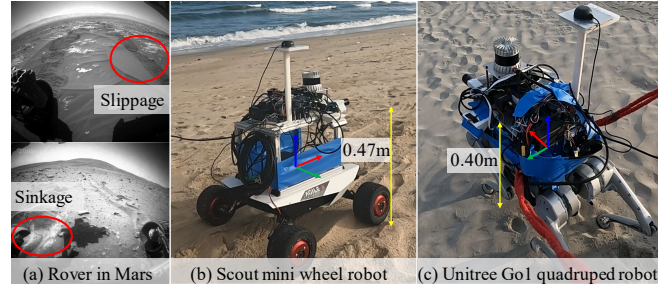


Fig. 1. (a) Terrain hazards encountered by NASA *Spirit* rover [4]. To study terrain-related hazards, we build a versatile sensor suite to record different data sequences in challenging soft, granular terrains. Both (b) wheeled robot and (c) quadruped robot platforms are used for carrying the designed sensor suite during terrain traversals of diverse sandy terrains, where robot locomotion can become quite challenging in certain scenarios.

perception on deformable, granular terrains, allowing for the understanding of dynamic robot-ground interaction and enhancement of traversability [3]. Additionally, these sensors often vary in characteristics and can guarantee system redundancy in a complementary way. Recent research on critical multi-sensor SLAM has progressively emerged as a necessary tool for negotiating such challenging terrains.

In recent years, the growing demand for effective SLAM solutions [5] has prompted the development of multi-sensor datasets. These datasets offer fair and repeatable operational tools, serving as valuable resources for algorithm implementation, comparison, and validation. Additionally, they can effectively evaluate challenging scenarios to analyze the diverse robot characteristics and limitations of current SLAM techniques. Furthermore, they could help to reduce unnecessary financial and engineering requirements. Certain datasets also introduce novel sensors, challenging existing solutions and fostering further research potentials [6]. Consequently, the use of such datasets accelerates breakthroughs concerning accuracy, robustness, and computational performance, thereby validating and enhancing general robot autonomy.

A. Related Work

Over the past years, numerous SLAM datasets, employing both simple and multi-sensor configurations, have been actively developed, covering structured and unstructured scenarios with unique robots, such as terrain hazards [20].

Several datasets were collected using single or simple sensor combinations, such as inertial measurement units (IMU), global positioning systems (GPS), cameras, and light detection and ranging (LiDAR). Notably, LiDAR-inertial odometry (LIO) and Visual-inertial odometry (VIO) are designed to fuse cameras or LiDAR data with inertial measurements

TABLE I
COMPARISON WITH VARIOUS NOTABLE PUBLIC DATASETS.

Dataset	Platform	Environments	Sensors						Sync.	GT Pose	
			IMU	LiDAR	GPS	Frame Cam.	Down'd RGBD Cam.	Robot Status			
EuRoc [7]	MAV	Indoors	✓			✓			Hw	Mocap/LT	
KAIST [8]	Car	Outdoors-Urban	✓	✓					\	SLAM	
KITTI [9]	Car	Outdoors-Urban	✓	✓	✓	✓			Hw/Sw	RTK-GPS	
M2DGR [10]	UGV	Campus/Lab	✓	✓	✓	✓			Sw	RTK-GPS/LT/Mocap	
FusionPortable [11]	Handheld/QR/UGV	In/Outdoors	✓	✓	✓	✓			Hw	Mocap/RTK-GPS/SLAM	
VECTOR [12]	Handheld/hemelet	Indoors	✓	✓		✓			Hw	MoCap + SLAM	
SubT-MRS [13]	Handheld/QR/UGV/MAV	In/Outdoors	✓	✓		✓			Hw	Super Odometry [14]	
Wild-Places [15]	Handheld	Outdoors-Jungle	✓	✓		✓			Hw	Wildcat SLAM [16]	
DiTer [17]	QR	Outdoors	✓	✓	✓	✓			\	RTK-GPS	
MADMAX [18]	UGV	Outdoors-Desert	✓		✓	✓		✓	Partial	RTK-GPS	
Katwijk [19]	Rover	Outdoors-Beach	✓	✓	✓	✓		✓	Hw/Sw	RTK-GPS	
Ours (TAIL)	UGV/QR	Soft terrains	✓	✓	✓	✓		✓	✓	Hw	RTK-GNSS

RTK: Real-time kinematic. QR: Quadraped robot. Mocap: Motion capture system. LT: Laser tracker. Sw/Hw: software/hardware synchronization. Down'd: Downward.

to improve the robustness and accuracy of localization. For example, EuRoc dataset [7] tracked a drone in both room and industrial environments. KAIST [8] presented an urban car dataset to capture the genuine features in areas where GPS signals show apparent degradation. However, these limited data could not capture full challenges in practice.

Several multi-sensor datasets are obtained in structured or semi-structured environments to address challenges. KITTI dataset [9] presented extensive car driving tasks to explore different perception scenes. M2DGR dataset [10] employed a ground robot to record different challenging scenarios. FusionPortable [11] proposed a campus-scene dataset tailored for evaluating SLAM across multi-platforms. VECTOR dataset [12] covered indoor scenarios and served as a versatile benchmark for event-centric studies with different devices.

Moreover, multi-sensor datasets prove essential for implementation in unstructured fields characterized by complex and natural obstacles. SubT-MRS [13] showed their real-world collection of datasets obtained from Subterranean (SubT) environments, with a focusing theme on testing SLAM in multi-robot, multi-spectral-inertial, and multi-degraded scenarios. Wild-Places [15] introduced a large-scale dataset in natural unstructured environments captured through a handheld device. DiTer [17] presented a terrain dataset designed for ground mapping using a quadruped robot. MADMAX dataset [18] utilized a UGV in the Moroccan desert to record different visual-inertial sequences. Katwijk [19] described a multi-sensor dataset along the beach near Katwijk to emulate potential rover landing sites.

This paper focuses on multi-modal SLAM datasets in unstructured granular terrain environments (see Fig.1), where geometric features are sparse and terrain-aware technology plays a pivotal role. Tab. I reviews the representative datasets related to our work. We see that datasets focusing on deformable terrain traversals (MADMAX and Katwijk) only studied wheeled locomotion, while those considered legged robots (FusionPortable, SubT-MRS, and DiTer) did not investigate soft environments. These works consider unique platforms in real-world operations, which may not always yield highly feasible measurements. However, the provision of intrinsic profiles can indeed enhance dynamic interactions and handle locomotion challenges in a complementary way

[21]. These problems motivate us to develop a dataset for distinct wheeled and legged locomotion in soft terrains and benchmark SLAM solutions with multiple sensory configurations. We expect that our dataset will provide significant advancements to bridge the gap in multi-sensor fusion within the SLAM and field robotics research community.

B. Contributions

We create the **Terrain-Aware Multi-Modal (TAIL)** dataset, a viable and promising SLAM dataset for both wheeled and legged robots traveling dynamically in deformable, granular scenarios, as described in Fig. 1. The main purpose of TAIL is to propel the development of multi-sensor fusion SLAM techniques in soft terrains, which can capture the distinct heterogeneous proprioception and exteroception. Specially, it exhibits various kinematic patterns and multiple sandy terrestrial interaction to challenge SLAM algorithms.

Our main contributions are listed as follows:

- We construct the TAIL dataset, which packages a versatile and hardware-synchronized sensor suite capable of millisecond-level and adjustable time intervals, comprising comprehensive sensors, a processor, and a battery (Fig. 2). This device can serve as an experimental tool for algorithm evaluation on sandy terrains.
- We collect the TAIL sequences with rich info. covering a wide spectrum of field complexities (texture-less), scope (surrounding and ground-pointing), and scene changes (illumination, moving objects, and flowing sands) faced in two types of soft sands. Notably, we are the first to present distinct proprioception for wheeled and quadruped robots that can capture distinct motion interaction within two changeable sandy scenes.
- We conduct algorithm validation using the TAIL dataset to benchmark representative state-of-the-art (SOTA) SLAM algorithms. The results indicate that multi-terrains and distinct robot locomotion modes pose additional challenges to SLAM, emphasizing the need for heightened attention in designing sensor fusion SLAM.

The rest of this paper is organized as follows: Sec. II introduces the sensor suite system. The detailed features of the dataset sequences are outlined in Sec. III. In Sec. IV, we benchmark the performance of various SLAM algorithms. Conclusion and future work are discussed in Sec. V.

TABLE II
OVERVIEW OF THE HARDWARE SPECIFICATIONS USED IN THE MULTI-SENSOR DEVICE

Hardware	Type	Characteristics	Rate	Topic name	Topic type
3D LiDAR	Ouster OS0-128	128×2048 points, 50m range. ±1.5-5cm range precision. FOV: 90°V/360°H. IMU: ICM20948,100Hz, 9-axis MEMS.	10Hz	/ouster/points /ouster/nearir_image /ouster/range_image /ouster/reflec_image /ouster/signal_image /ouster/imu	sensor_msgs/PointCloud2 sensor_msgs/Image sensor_msgs/Image sensor_msgs/Image sensor_msgs/Image sensor_msgs/Imu
Frame Cameras	2× HKVision MV-CA013-A0UC	1280×1024 pixels, global shutter. FOV: 66.5°vert., 82.9°horiz., >53dB.	30Hz	/left_camera/image/compressed /right_camera/image/compressed	sensor_msgs/CompressedImage sensor_msgs/CompressedImage
RGB-D Camera	Azure Kinect DK	1280×720 pixels, time-of-flight. FOV: 65°V/75°H. 0.5-3.86m. Depth: 640×576 pixels Intrinsic calibrated. Ground-level view.	30Hz	/depth/camera_info /depth/image_raw /depth/points /rgb/camera_info /rgb/image_raw/compressed	sensor_msgs/CameraInfo sensor_msgs/Image sensor_msgs/PointCloud2 sensor_msgs/CameraInfo sensor_msgs/CompressedImage
RGB-D Camera	2× Intel Realsense D435i	640×480 pixels, HD 16:9. 0.3-3.0m. FOV: 58°V/85.2°H. Only depth camera is synchronized. Depth: 848×480 pixels Intrinsic calibrated. Ground-level view.	15Hz	/D435_left/color/camera_info /D435_left/color/image_raw/compressed /D435_left/depth/camera_info /D435_left/depth/image_rect_raw /D435_right/color/camera_info /D435_right/color/image_raw/compressed /D435_right/depth/camera_info /D435_right/depth/image_rect_raw	sensor_msgs/CameraInfo sensor_msgs/CompressedImage sensor_msgs/CameraInfo sensor_msgs/Image sensor_msgs/CameraInfo sensor_msgs/CompressedImage sensor_msgs/CameraInfo sensor_msgs/Image
IMU	XSens MTi-680G	Roll/Pitch: 0.2° RMS, Yaw: 0.5° RMS. Pos: 1cm+1ppm CEP, Vel: 0.05m/s RMS.	100Hz	/imu/data	sensor_msgs/Imu
RTK	Ublox ZED-F9P	6 DoF ground truth. INS: 9-axis Localization accuracy 2cm.	100Hz 1Hz	/filter/positionlla /status	geometry_msgs/Vector3Stamped diagnostic_msgs/KeyValue
Robot platforms	Scout Mini	4WD, 6 DOF wheel odometry. Kinematic profiles, motor, driving status	50Hz	/cmd_vel /odom /scout_status	geometry_msgs/Twist nav_msgs/Odometry scout_msgs/ScoutStatus
	Unitree-GO 1	6 DOF leg odometry. Kinematic profiles, motor, gait, foot status	500Hz	/high_state	unitree_legged_msgs/HighState

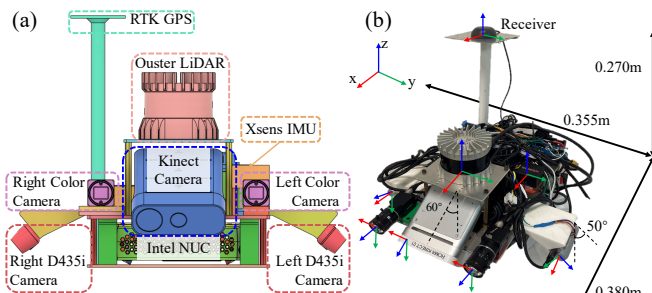


Fig. 2. The specification for the multi-modal sensor suite. (a) CAD model and hardware components of the setup. (b) The mounted device’s size and relevant coordinate frames of the sensor system. High-resolution 3D LiDAR is located at the center and an RGBD camera is installed below. Two frames and RGBD cameras are mounted on the left and right sides, complemented by an internally placed high-precision IMU and a rear-installed RTK-GPS. All these sensors are mounted on the same rigid aluminum frame and can be mounted on various robot platforms, e.g., see Fig. 1. Thus, their spatial relations have no deviation, making it an effective test tool.

II. SYSTEM OVERVIEW

This section introduces the sensor suite configuration and provides detailed information on its hardware time synchronization and spatial-temporal calibration. Fig. 2 depicts the suite setup, with different sensors securely fastened to the supporting frame that can be mounted on different robots.

A. Sensor Setup

We summarize the characteristics with corresponding messages for these sensor components in Tab. II. All sensor drivers are implemented on an Intel NUC running Ubuntu

20.04 LTS and the Robot Operation System (ROS) Noetic system. It is equipped with an i9 processor, a GeForce GTX 2060 GPU, 64GB DDR4 memory, and 2TB SSD.

1) *Inertial Measurement Unit*: We rigidly place the 9-axis IMU (model: XSens MTi-680G) at the rear as the main inertial sensor. Configured to operate at a high rate of 100Hz, it provides low-drift data, effectively mitigating unexpected motion measurements.

2) *3D LiDAR*: We place the OS0-128 LiDAR on top of the suite to measure the large 3D surrounding environments. We use four standoffs to raise the LiDAR’s height to prevent possible obstruction of the bottom laser beams. Operating at 10Hz, the LiDAR can output 1028×128 near-IR images, range images, reflected images, and signal images, which correlate with point clouds of the same scenes. Additionally, the LiDAR’s internal IMU can also output the linear accelerations and angular velocities at a rate of 100Hz.

3) *Regular Stereo Frame Cameras*: A pair of HKVision MV-CA013-A0UC global-shutter color cameras are mounted as a forward-looking stereo camera system. The horizontal baseline is approximately 16.7mm. Each camera is paired with an MVL-HF0824M-10MP lens, offering a 62.46°×44.05° field of view (FOV). We set their exposure time as fixed values to reduce relative latency.

4) *RGB-D Cameras*: The Kinect Azure DK camera is installed in the middle of the suite, obtaining sufficient ground views by employing the unbinned narrow-FOV depth mode. In addition, two Intel RealSense D435i RGB-D cameras are arranged on the side to enhance terrestrial observations. Note that only the depth streams are synchronized for D435i

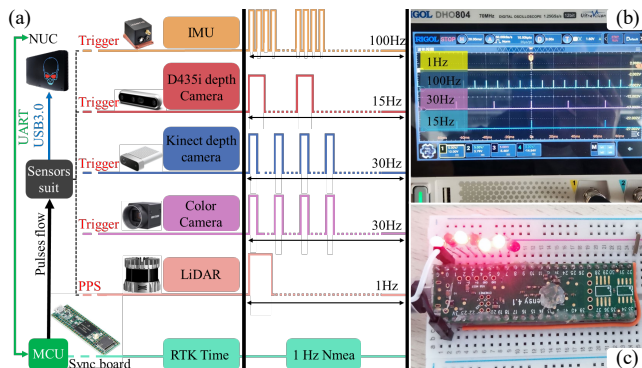


Fig. 3. The description of sensor hardware time synchronization process. (a) Triggering implementation using different marked signals. (b) Visualization of the triggering pulses on the oscilloscope. (c) Validating the accuracy of hardware triggering using the Light Emitting Diode (LED) board.

cameras while their color cameras use the rolling shutter mechanism. The arrangement of the three RGB-D cameras ensures a large perception FOV to form a ground-looking measurement system. Notably, the RGB-D cameras measure short-range, small-scale ground scenarios, while the LiDAR measures larger-scale surrounding scenarios.

5) *RTK*: An IMU-configured ZED-F9P RTK is employed, with its receiver installed at the rear of the sensor suite. It provides GNSS-IMU integrated trajectory readings¹ in the World Geodetic System 84 (WGS 84) reference frames.

6) *Robot Platforms*: Additionally, we capture the internal motion status of the robot, accounting for its specific mobility when navigating different locations with varying terrains. The message types are custom definitions for the wheeled robot Scout mini² and the quadruped robot Unitree Go1³. The robot profile encompasses built-in kinematics, odometry, and driving data, etc. The wheeled robot employs high-speed CAN, while the legged robot utilizes Ethernet, linking to the NUC computer to ensure low-latency communication.

B. Time Synchronization

We synchronize all sensors in the sensor suite at the hardware level to capture real-time data through the trigger signal in Fig.3(a)(b). We employ a Teensy 4.1 as the microcontroller unit (MCU) [22]. It can obtain the National Marine Electronics Association (NMEA) pulse per second (PPS) signal from the RTK receiver to synchronize the ROS time from the GPS time. To enhance the scalability of the hardware trigger system and mitigate response time variations among different cameras, the MCU generates 12 channels of trigger pulses at 3.3V. Configuration of the frequency and time offset for these triggering pulses is adjustable through a serial debugging assistant on the host computer. Furthermore, all trigger signals are accurately aligned to the PPS signal, exhibiting a precision of less than 1 microsecond.

¹https://github.com/jiminghe/Xsens_MTi_ROS_Driver_and_Ntrip_Client

²https://github.com/agilexrobotics/scout_ros/tree/master/scout_msgs/msg

³https://github.com/unitreerobotics/unitree_ros_to_real/tree/master/unitree_legged_msgs/msg

TABLE III
SPECIFICATION OF CALIBRATION PROCESS

Calibration Item	Methods
Intrinsic of IMU	Allan Variance ROS
Intrinsic of Color Cameras	ROS camera calibration
Stereo frame Cameras Extrinsic	Stereo Camera
Color Camera-IMU Extrinsic	Kalibr
Kinect Color Camera-LiDAR Extrinsic	MATLAB

Upon receiving a start/configuration pulse-per-second (PPS) signal from the RTK, the MCU dynamically programs various preconfigured trigger signals for the LiDAR, D435i cameras, Kinect, stereo frame cameras, and IMU. The LiDAR's internal clock is synchronized through the PPS, initiating the capture of individual scans triggered by a 1Hz signal. Following a 15Hz trigger pulse, only the depth camera in the RGB-D D435i is directly activated, while the color camera achieves data synchronization with the depth camera through its built-in software synchronization. The stereo frame cameras are triggered by a 30Hz signal, activating the global shutter for the predetermined exposure duration. The same 30Hz signal is also forwarded to the Kinect camera. Additionally, the IMU is triggered by a sequence of 100 pulses at 10ms intervals via rising edges. When receiving an end trigger signal from the command, all aforementioned signals, except PPS (from RTK), are terminated.

To assess the precision of sensor hardware synchronization, we conducted a flashing experiment depicted in Figure 3(c). The MCU receives the PPS signal from RTK and generates seven channels of 1Hz pulses with a rising edge width of 0.45ms to drive LED flashes. To achieve a continuous change in the states of the LED captured by the cameras, the LED flashes sequentially in a 7-bit binary pattern, with each LED remaining illuminated for a duration of less than 0.45ms. Multiple cameras can capture the LED light with the same binary state simultaneously, which indicates that the accuracy of our customized synchronization module can reach the millisecond level.

C. Sensor Calibration

Table. III shows the illustration of all calibration variables and their calibration sequence. Initially, the intrinsic parameters of each sensor are calibrated, followed by the estimation of extrinsics parameters with fixed intrinsics to establish spatial correlation. We define the coordinate system of the Xsens IMU as the *reference frame* where extrinsics of other sensors are referred to.

1) *Intrinsics calibration*: We calibrate the IMU intrinsic using the Allan Variance ROS toolbox⁴ and all the color cameras' intrinsic of pinhole models by the ROS camera calibration toolbox⁵.

2) *Extrinsics calibration*: We identify the spatial-temporal parameters between different color cameras with the Xsens IMU using the Kalibr toolbox⁶. Note only the extrinsic between Xsens IMU concerning the color cameras are

⁴https://github.com/ori-drs/allan_variance_ros

⁵http://wiki.ros.org/camera_calibration

⁶<https://github.com/ethz-asl/kalibr>



Fig. 4. Sampled challenging scenarios shows the in-sequence diversity. We capture a variety of terrain characteristics with stereo frame cameras, three RGB-D cameras, and LiDAR.



Fig. 5. Overview of our field experiments for the TAIL data collection. (a) Acquisition locations are depicted on the satellite map. (b) Coarse, steep beach from shanhaili. (c) Fine, smooth beach from wanke.

calibrated and defined as: $\langle \text{Xsens, frame cameras} \rangle$, $\langle \text{Xsens, D435i color cameras} \rangle$, $\langle \text{Xsens, Kinect color cameras} \rangle$. Additionally, we utilize the MATLAB toolbox⁷ to obtain the extrinsic for the Kinect color camera-LiDAR. The Stereo Camera toolbox⁸ is used for the stereo frame cameras.

Other sensors can be derived from the calibration chain and transformations, or appended using the pre-existing, factory calibration parameters. Additionally, we incorporate the distinct coordinate systems of the robot platforms into the primary chain based on information provided in the manufacturer’s manual. To aid future studies, we include Computer-Aided Design (CAD) measurements of all inter-sensor relative transformations for the actual assembly.

III. DATASET OVERVIEW

This section introduces the detailed collection of diverse sequences, which are set as the criteria of the TAIL dataset.

A. Dataset Scenarios

We provide 14 traveled sequences within the outdoor sites to test the performance of SLAM algorithms under various levels of challenges. Two specific locations on the beaches of Double Moon Bay (22°N, 114°E), known as shanhaili and wanke, are selected as our field analog sites since they are natural, unstructured, and sandy with

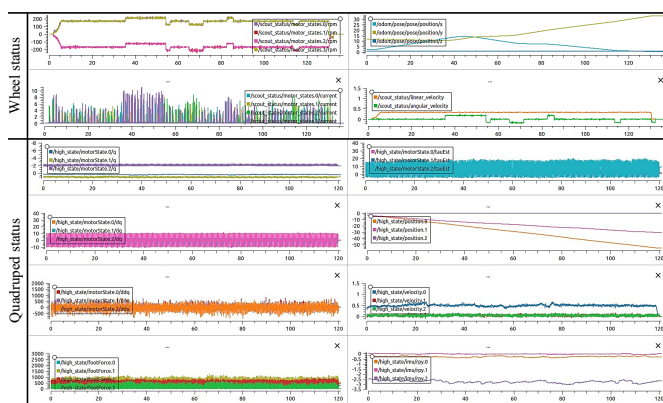


Fig. 6. Visualization of different inertial kinematic parameters from wheeled and quadruped robots.

distinct size in widely-open areas. Fig. 5 reveals the filed scenarios for the diverse traverses, which have individual unique geological characteristics. Additionally, Fig. 4 shows sensor measurements obtained from wheel and quadruped platforms in different scenarios. Tab. IV concludes and describes the features of each sequence. Note both types of robot inertial kinematic status are collected, including dynamic motions under different types of terrain conditions. The characteristics are categorized as follows:

- 1) **Terrains:** Unstructured terrains can be found in coarse and fine sand benches, mainly ranging from easily traversable areas to sloped areas that are hard to cross. The granular mediums in such terrains have distinct particle sizes and specific mechanical properties, which influence SLAM with ground interaction [23], [24].
- 2) **Surface appearance:** Granular sands tend to exhibit low saliency features and lack texture, which can influence visual analysis. Moreover, the grassy, dry/wet sands offer a greater variety of ground features.
- 3) **Illumination:** Color cameras are sensitive to lighting conditions, especially when the robot moves backlight or encounters issues such as underexposure or strong exposure. Such motions would negatively affect the visual processing algorithms.

⁷<https://www.mathworks.com/help/lidar/ug/lidar-and-camera-calibration.html>

⁸<https://www.mathworks.com/help/vision/ug/using-the-stereo-camera-calibrator-app.html>

TABLE IV
OVERVIEW OF DATASET SEQUENCES

Platforms	Locations	Motions	Sequences Description	Seq.	T[s]	$ \bar{v} $ [m/s]	L[m]	Lighting	Appearance	Objects	Size[GB]
Wheeled Robot	shanhaili	slow	backward, planar	1	162	0.4	63.1	weak	grassy, coarse sand	static	21.8
		medium	forward, planar	2	177	0.5	87.0	normal	coarse sand	static	21.3
		fast	forward, planar	3	105	0.8	81.3	normal	coarse sand	static	12.3
	wanke	slow	forward, planar	4	142	0.1	15.0	weak	fine sand	static	17.0
		slow	backward, planar	5	137	0.3	39.7	normal	grassy, fine sand	static	17.2
		slow	backward, planar	6	137	0.3	37.6	normal	fine sand	dynamic	15.1
		medium	backward, planar	7	145	0.4	58.5	normal	fine sand	static	16.3
		fast	forward, planar	8	176	0.8	148.5	strong	fine sand	static	19.3
Quadruped Robot	shanhaili	slow	forward, planar, jerky	9	153	0.4	58.9	weak	coarse sand	static	17.4
		fast	forward, planar, jerky	10	74	0.5	37.1	weak	coarse sand	static	8.5
	wanke	slow	forward, planar, jerky	11	144	0.3	49.6	strong	fine sand	static	15.1
		fast	forward, planar, jerky	12	148	0.7	103.3	strong	fine sand	static	15.1
		fast	backward, planar, jerky	13	175	0.3-0.7	69.4	normal	fine sand	dynamic	19.3
		fast	Multiple loops, planar, jerky	14	194	0.5	90.5	normal	fine sand	static	21.3

Seq. means sequences. $||\bar{v}||$ means the commanded linear velocity. L means the total traveling distance. T means total time.

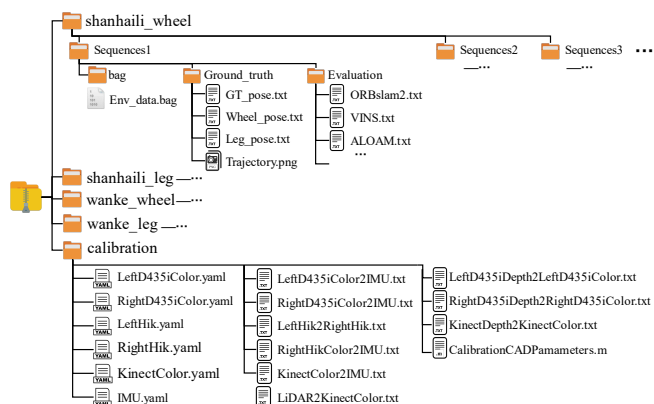


Fig. 7. Structure of the TAIL dataset. In each package, the sequence is named as the observed environmental and the recorded date: `env_date`. Ground-truth poses, odometry, and estimated trajectories are also contained.

- 4) **Dynamic objects:** Moving objects inevitably affect perception performance and leave “ghostly shadows” [25], [26], which can not be treated as static background data for both visual and LiDAR perception.
- 5) **Multiple loops:** Multiple loop trajectories are tested by driving in a circular path several times, which can help validate the accuracy of the odometry.
- 6) **Motion patterns:** Different motion patterns (low, medium, high speeds) can result in significant camera blur and terrain hazards [22], [27]. The corresponding kinematic parameters regarding different robot motions can be seen in Fig. 6. Moreover, wheeled robots exhibit planar motions while quadruped robots perform planar but jerky motions on granular sand. Such robotic interaction provides a complement of heterogeneous proprioception information for exteroception perception.

B. Ground Truth

We provide 6-DoF (Degree of Freedom) reference ground truth for each sequence to evaluate the SLAM in soft terrains, which is obtained by the IMU-integrated RTK measurements. As SLAM methods represent poses concerning an arbitrary initial starting frame, we transform the pose trajectories obtained from diverse SLAM readings and IMU-integrated RTK into the LiDAR frame using extrinsic parameters. The aligned trajectories serve as a means of comparing the results with the ground truth for the latter evaluation in Sec. IV.

C. Dataset Formats

Fig. 7 details the structure of TAIL dataset. The simultaneously collected sensor data is stored in the format of a set of individual rosbags in corresponding sequences-*i*, which can be processed using ROS tools. Timestamps for all messages are derived from their publication time on ROS and can be found in the `header.stamp` field. Each sub-package is named after the observed sites and a postfix indicating the different motion configuration (`shanhaili_wheel`, `shanhaili_leg`, `wanke_wheel`, and `wanke_leg`). It also provides ground-truth trajectories with robotic pose for benchmarking and validation purposes. Moreover, the data evaluation files are shown to process the measurements with different SLAM algorithms. Additionally, the dataset includes calibration files and frame relationships derived from CAD measurements.

IV. EXPERIMENT

To validate the versatility of the proposed datasets, we conduct a benchmarking study on several SOTA SLAM systems and report their results. The robots’ internal odometry and the following open-source algorithms using diverse sensor combinations and technologies are evaluated: ORB-SLAM2 (right D435i color cameras) [28], VINS-Fusion (IMU+left frame camera) [29], A-LOAM (LiDAR-only) [30], FAST-LIO2 (IMU+LiDAR) [31], and FAST-LIVO (IMU+LiDAR+left frame camera) [32]. The default parameter configuration files are rectified to fit our sequences and also released. We use `EVO`⁹ with the Technical University of Munich (TUM) format (time, x,y,z,qx,qy,qz,qw) to analyze pose accuracy. The mean absolute trajectory error (ATE) and relative trajectory error (RTE) of estimation in the translation part are calculated w.r.t. the ground truth. Tab. V summarizes the quantitative localization results, while Fig. 8 visualizes the estimated trajectories.

Our TAIL dataset can support a wide range of autonomy frameworks that vary significantly, including mono, visual-inertial, LiDAR-only, LiDAR-inertial, LiDAR-visual-inertial fusions, and robot odometry. These frameworks also demonstrate the quality of our synchronization and calibration.

⁹<https://github.com/MichaelGrupp/evo>

TABLE V
PERFORMANCE COMPARISON OF SOTA SLAM ALGORITHMS ON OUR DATASET

Platforms	Locations	Seq.	Odometry		ORB-SLAM2		VINS		VINS-Loop		A-LOAM		FAST-LIO2		FAST-LIVO	
			RPE	ATE	RPE	ATE	RPE	ATE	RPE	ATE	RPE	ATE	RPE	ATE	RPE	ATE
Wheeled Robot	shanhaili, coarse sand	1	0.008	0.548	0.020	2.472	0.135	2.678	0.091	2.666	0.025	0.360	0.018	0.287	0.024	0.554
		2	0.005	14.174	0.014	5.412	0.018	6.034	0.041	5.582	0.050	1.796	0.021	0.799	0.017	0.950
		3	0.008	15.242	×	×	×	×	×	×	0.089	10.486	0.043	1.282	0.063	3.138
	wanke, fine sand	4	0.001	1.056	0.008	0.135	0.008	3.774	0.200	3.538	0.011	0.307	0.008	0.333	0.008	0.323
		5	0.003	2.068	0.010	0.923	0.006	1.013	0.021	0.887	0.017	0.911	0.010	0.929	0.015	0.896
		6	0.002	5.015	0.009	0.889	0.084	7.754	0.089	8.076	0.017	0.814	0.011	0.879	0.017	0.838
		7	0.002	1.887	0.017	3.291	0.061	4.207	0.225	3.891	0.017	1.406	0.011	1.441	0.011	1.336
		8	0.005	27.774	×	×	0.032	11.556	0.091	8.578	0.029	3.008	0.014	3.215	0.024	3.021
Quadruped Robot	shanhaili, coarse sand	9	0.010	1.623	×	×	×	×	×	0.102	2.250	0.089	5.982	0.074	2.942	
		10	0.011	0.828	×	×	×	×	×	0.083	4.982	×	×	0.197	9.598	
	wanke, fine sand	11	0.007	1.263	×	×	×	×	×	0.041	0.737	0.067	1.201	0.140	0.758	
		12	0.014	3.076	×	×	×	×	×	0.047	2.263	0.022	2.557	0.032	2.334	
		13	0.009	2.486	×	×	×	×	×	0.038	1.334	0.023	1.559	0.026	1.453	
		14	0.009	0.597	×	×	×	×	×	0.117	6.873	0.150	27.942	0.166	31.553	

"Loop" means that the loop closure is considered. "×" means that the method fail in this sequence.

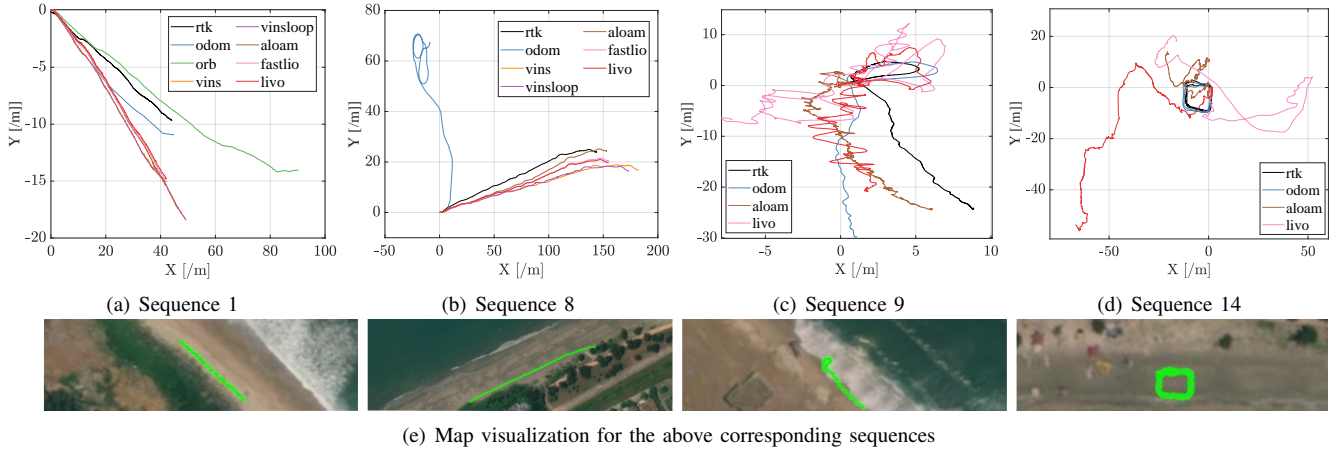


Fig. 8. Comparison of estimated trajectories with respect to the ground truth in four representative data sequences.

The TAIL dataset can serve as a rigorous test bench and the ATE results are used as a baseline to elucidate inherent shortcomings. LiDAR-based methods generally outperform vision-based methods when operating in fine terrains. Both methods, however, are prone to failure due to sensor degradation. ORB-SLAM2 and VINS-Fusion fail in some wheel robot driving cases and all quadruped robot traveling cases (8/14 tests fail). These failures occur when the scenes have dark or dynamic images while the scenes are texture-less, leading to poor initialization. Additionally, image blurring and the rolling shutter effect induced by the robot's aggressive movement in deformable terrains adversely impact visual detection. A-LOAM performs better in sequences involving travel on fine sand, capitalizing on LiDAR's enhanced perception capabilities, but it struggles in coarse terrains. Although FAST-LIO2 has a remarkable performance with the aid of the IMU, it occasionally produces unreliable results in certain sequences, particularly when used with quadruped robots as the unreliable sensors' measurements. FAST-LIVO exhibits greater robustness but does not perform well in localization accuracy, even in slow sequences involving wheel robots where the multi-modal features are prone to failure in such texture-less terrains. Conversely, leg odometers ensure reliable operation in select quadruped locomotion sequences. These sequences have high textural monotonicity and severe vibrations rendering visual-

based methods ineffective, indicating limited robustness in multi-degraded environments.

The results indicate that the integration of multiple sensors is essential for achieving high accuracy and robustness in complex environments, particularly when considering the internal kinematic parameters. In general, this dataset may not be a perfect collection [33], but it provides valuable real-world scenarios encountered by various types of robot platforms. These scenarios can serve as performance tests, feasibility references, and representative comparisons for evaluating sensor fusion mechanisms. The TAIL dataset highlights the necessity of applying advanced SLAM techniques in the real-world for the research community. We hope that TAIL will contribute to the advancement of autonomous robots by providing timely and complementary scene data.

V. CONCLUSION

This paper presents TAIL, a novel terrain-aware multi-modal dataset targeting the development of SLAM algorithms capturing unique wheel and legged motion when traveling over two dynamic sandy scenes. The comprehensive data collection in the wilds allows TAIL to examine the scenes on surrounding and supporting ground, track scene changes, analyze the motion proprioception of these platforms, and enhance understanding of robotic-centric terrain interactions. We benchmark SOTA SLAM algorithms using

our dataset with ground truth and identify additional challenges to be tackled for robot navigation over soft terrains.

In the future, we plan to periodically update and extend this dataset to include more comprehensive and challenging environments, covering more real-world scenarios that can contribute to the development of multi-sensor fusion SLAM within distinct robots. Additionally, we intend to explore more terrain-aware tasks, including terrain segmentation, ground interaction and motion estimation for different autonomous robots in different terrains.

ACKNOWLEDGMENT

The authors express their sincere gratitude to the technicians from Ouster and Xsens for their valuable assistance in the project's progress. Moreover, we appreciate the open-source methods and the members of FusionPortable [11] and VECtor [12], which facilitate the development of our proposed framework.

REFERENCES

- [1] G. Webster and V. McGregor, "Nasa's mars rover has uncertain future as sixth anniversary nears," 2009. [Online]. Available: <https://mars.nasa.gov/mer/newsroom/pressreleases/20091231a.html>
- [2] R. A. Kerr, "Mars rover trapped in sand, but what can end a mission?" *Science*, vol. 324, no. 5930, pp. 998–998, 2009.
- [3] D. D. Fan, K. Otsu, Y. Kubo, A. Dixit, J. Burdick, and A.-A. Agha-Mohammadi, "Step: Stochastic traversability evaluation and planning for risk-aware off-road navigation," in *Robotics: Science and Systems XVII*. Robotics: Science and Systems Foundation, 2021.
- [4] M. Smith, I. Baldwin, W. Churchill, R. Paul, and P. Newman, "The new college vision and laser data set," *The International Journal of Robotics Research*, vol. 28, no. 5, pp. 595–599, 2009.
- [5] T. Shan, B. Englot, C. Ratti, and D. Rus, "Lvi-sam: Tightly-coupled lidar-visual-inertial odometry via smoothing and mapping," in *2021 IEEE International Conference on Robotics and Automation (ICRA)*. IEEE, 2021, pp. 5692–5698.
- [6] E. Mueggler, H. Rebecq, G. Gallego, T. Delbruck, and D. Scaramuzza, "The event-camera dataset and simulator: Event-based data for pose estimation, visual odometry, and slam," *The International Journal of Robotics Research*, vol. 36, no. 2, pp. 142–149, 2017.
- [7] M. Burri, J. Nikolic, P. Gohl, T. Schneider, J. Rehder, S. Omari, M. W. Achtelik, and R. Siegwart, "The euroc micro aerial vehicle datasets," *The International Journal of Robotics Research*, vol. 35, no. 10, pp. 1157–1163, 2016.
- [8] J. Jeong, Y. Cho, Y.-S. Shin, H. Roh, and A. Kim, "Complex urban lidar data set," in *2018 IEEE International Conference on Robotics and Automation (ICRA)*. IEEE, 2018, pp. 6344–6351.
- [9] A. Geiger, P. Lenz, C. Stiller, and R. Urtasun, "Vision meets robotics: The kitti dataset," *The International Journal of Robotics Research*, vol. 32, no. 11, pp. 1231–1237, 2013.
- [10] J. Yin, A. Li, T. Li, W. Yu, and D. Zou, "M2dgr: A multi-sensor and multi-scenario slam dataset for ground robots," *IEEE Robotics and Automation Letters*, vol. 7, no. 2, pp. 2266–2273, 2021.
- [11] J. Jiao, H. Wei, T. Hu, X. Hu, Y. Zhu, Z. He, J. Wu, J. Yu, X. Xie, H. Huang *et al.*, "Fusionportable: A multi-sensor campus-scene dataset for evaluation of localization and mapping accuracy on diverse platforms," in *2022 IEEE/RSJ International Conference on Intelligent Robots and Systems (IROS)*. IEEE, 2022, pp. 3851–3856.
- [12] L. Gao, Y. Liang, J. Yang, S. Wu, C. Wang, J. Chen, and L. Kneip, "Vector: A versatile event-centric benchmark for multi-sensor slam," *IEEE Robotics and Automation Letters*, vol. 7, no. 3, pp. 8217–8224, 2022.
- [13] S. Zhao, D. Singh, H. Sun, R. Jiang, Y. Gao, T. Wu, J. Karhade, C. Whittaker, I. Higgins, J. Xu, Y. Qiu, S. Saha, C. Wang, W. Wang, and S. Scherer, "Subt-mrs: A subterranean, multi-robot, multi-spectral and multi-degraded dataset for robust slam," 2023.
- [14] S. Zhao, H. Zhang, P. Wang, L. Nogueira, and S. Scherer, "Super odometry: Imu-centric lidar-visual-inertial estimator for challenging environments," in *2021 IEEE/RSJ International Conference on Intelligent Robots and Systems (IROS)*. IEEE, 2021, pp. 8729–8736.
- [15] J. Knights, K. Vidanapathirana, M. Ramezani, S. Sridharan, C. Fookes, and P. Moghadam, "Wild-places: A large-scale dataset for lidar place recognition in unstructured natural environments," in *2023 IEEE International Conference on Robotics and Automation (ICRA)*. IEEE, 2023, pp. 11 322–11 328.
- [16] M. Ramezani, K. Khosoussi, G. Catt, P. Moghadam, J. Williams, P. Borges, F. Pauling, and N. Kottege, "Wildcat: Online continuous-time 3d lidar-inertial slam," *arXiv preprint arXiv:2205.12595*, 2022.
- [17] S. Jeong, H. Kim, and Y. Cho, "Diter: Diverse terrain and multi-modal dataset for field robot navigation in outdoor environments," in *2023 IEEE International Conference on Robotics and Automation (ICRA) Workshop*, 2023.
- [18] L. Meyer, M. Smířek, A. Fontan Villacampa, L. Oliva Maza, D. Medina, M. J. Schuster, F. Steidle, M. Vayugundla, M. G. Müller, B. Rebele *et al.*, "The madmax data set for visual-inertial rover navigation on mars," *Journal of Field Robotics*, vol. 38, no. 6, pp. 833–853, 2021.
- [19] R. A. Hewitt, E. Boukas, M. Azkarate, M. Pagnamenta, J. A. Marshall, A. Gasteratos, and G. Visentin, "The katwijk beach planetary rover dataset," *The International Journal of Robotics Research*, vol. 37, no. 1, pp. 3–12, 2018.
- [20] J. G. Rogers, J. M. Gregory, J. Fink, and E. Stump, "Test your slam! the sub-tunnel dataset and metric for mapping," in *2020 IEEE International Conference on Robotics and Automation (ICRA)*. IEEE, 2020, pp. 955–961.
- [21] C. Yao, G. Shi, Z. Zhu, and Z. Jia, "Staf: Interaction-based design and evaluation of sensorized terrain-adaptive foot for legged robot traversing on soft slopes," in *IEEE/ASME Transactions on Mechatronics*. IEEE, 2023, minor revision.
- [22] G. Shi, C. Yao, W. Wang, Z. Zhu, and Z. Jia, "Adaptive planar foot with compliant ankle joint and multi-modal sensing for quadruped robots," in *2022 IEEE International Conference on Robotics and Biomimetics (ROBIO)*. IEEE, 2022, pp. 52–57.
- [23] C. Yao, F. Xue, Z. Wang, Y. Yuan, Z. Zhu, L. Ding, and Z. Jia, "Wheel vision: Wheel-terrain interaction measurement and analysis using a sensorized transparent wheel on deformable terrains," *IEEE Robotics and Automation Letters*, vol. 8, no. 12, pp. 7938–7945, 2023.
- [24] F. Xue, C. Yao, Y. Yuan, Y. Ge, W. Shi, Z. Zhu, L. Ding, and Z. Jia, "Wheel-terrain contact geometry estimation and interaction analysis using aside-wheel camera over deformable terrains," *IEEE Robotics and Automation Letters*, vol. 8, no. 11, pp. 7639–7646, 2023.
- [25] C. Yao, H. Zhu, S. Lv, D. Zhang, and Z. Jia, "Robust method for static 3d point cloud map building using multi-view images with multi-resolution," in *2021 IEEE International Conference on Real-time Computing and Robotics (RCAR)*. IEEE, 2021, pp. 782–787.
- [26] H. Zhu, C. Yao, Z. Zhu, Z. Liu, and Z. Jia, "Fusing panoptic segmentation and geometry information for robust visual slam in dynamic environments," in *2022 IEEE 18th International Conference on Automation Science and Engineering (CASE)*. IEEE, 2022, pp. 1648–1653.
- [27] C. Yao, G. Shi, Y. Ge, Z. Zhu, and Z. Jia, "Predict the physics-informed terrain properties over deformable soils using sensorized foot for quadruped robots," in *2023 International Conference on Advanced Robotics and Mechatronics (ICARM)*. IEEE, 2023, pp. 330–335.
- [28] R. Mur-Artal and J. D. Tardós, "Orb-slam2: An open-source slam system for monocular, stereo, and rgb-d cameras," *IEEE Transactions on Robotics*, vol. 33, no. 5, pp. 1255–1262, 2017.
- [29] T. Qin, S. Cao, J. Pan, and S. Shen, "A general optimization-based framework for global pose estimation with multiple sensors," *arXiv preprint arXiv:1901.03642*, 2019.
- [30] J. Zhang and S. Singh, "Loam: Lidar odometry and mapping in real-time," in *Robotics: Science and Systems*, vol. 2, no. 9. Berkeley, CA, 2014, pp. 1–9.
- [31] W. Xu, Y. Cai, D. He, J. Lin, and F. Zhang, "Fast-lio2: Fast direct lidar-inertial odometry," *IEEE Transactions on Robotics*, vol. 38, no. 4, pp. 2053–2073, 2022.
- [32] C. Zheng, Q. Zhu, W. Xu, X. Liu, Q. Guo, and F. Zhang, "Fast-livo: Fast and tightly-coupled sparse-direct lidar-inertial-visual odometry," in *2022 IEEE/RSJ International Conference on Intelligent Robots and Systems (IROS)*, 2022, pp. 4003–4009.
- [33] T.-M. Nguyen, S. Yuan, M. Cao, Y. Lyu, T. H. Nguyen, and L. Xie, "Ntu viral: A visual-inertial-ranging-lidar dataset, from an aerial vehicle viewpoint," *The International Journal of Robotics Research*, p. 02783649211052312, 2021.